Satiated relative permeability of variable-aperture fractures

Russell L. Detwiler
Lawrence Livermore National Laboratory, University of California, 7000 East Avenue, Livermore, California 94551, USA

Harihar Rajaram
Department of Civil, Environmental and Architectural Engineering, University of Colorado, 428 UCB, Boulder, Colorado 80309, USA

Robert J. Glass
Flow Visualization and Processes Laboratory, Sandia National Laboratories, Albuquerque, New Mexico 87185, USA
(Received 9 July 2004; revised manuscript received 27 December 2004; published 28 March 2005)

Experimental studies of capillary-dominated displacements in variable-aperture fractures have demonstrated the occurrence of a satiated state at the end of invasion, where significant entrapment of the displaced phase occurs. The structure of this entrapped phase controls the behavior of flow and transport processes in the flowing phase. Recent studies have shown that the areal saturation of the flowing phase at satiation (S_f) is largely controlled by a single parameter C/δ, where C, the curvature number, weighs the mean in-plane interfacial curvature relative to the mean out-of-plane interfacial curvature, and δ, the coefficient of variation of the aperture field, represents the strength of interface roughening induced by aperture variations. Here we consider the satiated relative permeability (k_{rs}) to the flowing phase, which is defined as the relative permeability when the defending phase is fully entrapped. The satiated relative permeability is shown to be a well-defined function of S_f over a wide range of C/δ, ranging from capillary fingering with significant entrapment ($C/\delta \rightarrow 0$) to smooth invasion with very little entrapment ($C/\delta > 1$). We develop a relationship for k_{rs} as a function of S_f, by combining theoretical results for the effective permeability in a spatially correlated random permeability field, with results from continuum percolation theory for quantifying the influence of the entrapped phase. The resulting model for k_{rs} also involves a dependence on δ. The predicted relative permeability values are accurate across the entire range of phase structures representative of capillary-dominated displacements in variable-aperture fractures.

DOI: 10.1103/PhysRevE.71.031114 PACS number(s): 46.65.+g, 47.55.Mh, 47.55.Kf, 47.54.+r

I. INTRODUCTION

The presence of two or more fluids within a fracture reduces the permeability to each phase [1–4]. This reduction in permeability is often represented by the relative permeability, which is the ratio of the permeability in two-phase flow to that in single-phase flow and varies between 0 and 1. Experiments and simulations have demonstrated that capillary-dominated displacements (i.e., negligible gravity and viscous forces) in statistically homogeneous variable-aperture fractures can result in a satiated condition in which the invading phase spans the fracture and the defending phase is completely entrapped [5–7]. The satiated state corresponds to the end of invasion (analogous to the second percolation threshold or trapping threshold defined by Wilkinson and Willemsen [5]), unlike the invasion percolation threshold, which corresponds to first breakthrough and spanning of the domain by the invading phase. The satiated state is established over relatively short time scales [6] and can persist within a variable-aperture fracture for a very long duration, unless disturbed by external forces [8] or dissolution of the entrapped phase [9,10]. The flow and transport properties corresponding to the satiated state are thus important to a variety of applied problems. In this paper, our objective is to develop a model for predicting the relative permeability under satiated conditions.

The satiated relative permeability (k_{rs}) is controlled by the geometry of the flowing phase at satiation, which is defined by the configuration of entrapped regions and the aperture variability induced by fracture surface roughness. During invasion, small perturbations in capillary forces along the invading interface, caused by local perturbations in interfacial curvature, lead to roughening of the interface and entrapment of the defending phase. The magnitude of interface roughening and the geometry of the resulting entrapped phase are controlled by aperture variability within the fracture and the contact angle between the invading and defending fluids at the rock surfaces. Invasion percolation (IP) algorithms, which have been widely used to simulate immiscible displacements in porous media [5,11,12] and fractures [13,14], sequentially fill sites with the largest value of

$$P_c = \Omega\left(\frac{1}{r_1} + \frac{1}{r_2}\right) \tag{1}$$

along the invading interface, where r_1 and r_2 are the two principal radii of interfacial curvature and Ω is the interfacial tension. In porous media, Eq. (1) is typically applied by assuming r_1 and r_2 are equal and proportional to the pore radius. In fractures, r_1 is measured orthogonal to the mean fracture plane (Fig. 1). Because r_2 is typically much larger than r_1, r_2 is often considered insignificant in determining invasion orders [13,14]. However, recent experimental studies [6] have demonstrated that in-plane interfacial curvature can lead to significant smoothing of interfaces. As a result,

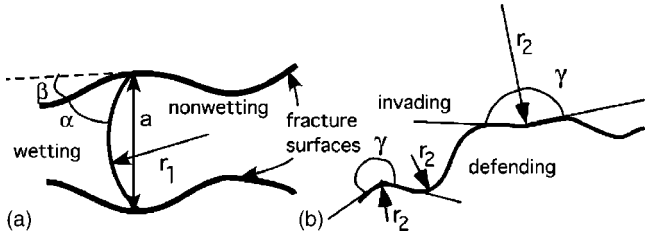

FIG. 1. Schematic of two fluid phases within a rough-walled fracture: (a) cross section defining the aperture-induced radius of curvature, r_1, local aperture a, contact angle α, and convergence-divergence angle β and (b) plan view (normal to fracture plane) defining the in-plane radius of curvature, r_2, and included angle γ (from invading phase).

phase geometries in two-phase flow through fractures can deviate significantly from the behavior predicted by IP algorithms.

A modified invasion percolation algorithm (MIP) that accounts explicitly for both r_1 and r_2 reproduces experimentally observed phase geometries better than IP [6]. For each iteration of the MIP algorithm, P_c is calculated at each location along the invading interface using (Fig. 1): $r_1 = a/2\cos(\alpha+\beta)$ and $r_2=(\lambda/2)\tan(\gamma/2)$, where a is the local fracture aperture, α is the fluid-fluid contact angle at the rock surfaces, β is the convergence-divergence angle of the opposing rock surfaces, γ is the included angle between two vectors that approximate the local interface from the invading fluid side, and λ is the correlation length of the variable aperture field; $\lambda/2$ is used here as a characteristic in-plane radius of curvature within a spatially correlated field. For small values of β and uniform α near 0 or π, we can neglect β and nondimensionalize Eq. (1) in terms of the parameter $C=\langle a\rangle/(\lambda\cos\alpha)$:

$$P_c^* = \frac{1}{r_1^*} + C\frac{1}{r_2^*}, \tag{2}$$

where the asterisk represents dimensionless variables (see Glass *et al.* [6] for details). In Eq. (2), C weighs the relative influences of mean in-plane and out-of-plane interfacial curvatures.

Recent theoretical and computational results based on MIP [15] demonstrate that a simple measure of the flowing phase structure at satiation, the areal saturation (S_f), depends strongly on the ratio of C and $\delta=\sigma_a/\langle a\rangle$, where $\langle a\rangle$ is the mean and σ_a the standard deviation of the aperture field, respectively. Thus, for any capillary-dominated invasion process in which values of $\langle a\rangle$, σ_a, λ, and α yield the same value of C/δ, the resulting entrapped-flowing phase structures will be similar. Effectively, C measures the strength of smoothing at the invading interface due to in-plane curvature, while δ measures the strength of roughening caused by random aperture variations, and it is the competition between these mechanisms that controls phase geometry. For C/δ well below 1, out-of-plane, aperture-induced curvature dominates, and the phase structure corresponds to IP within a spatially correlated field. As C/δ increases, capillary fingers widen to above the spatial correlation length, due to smoothing generated by in-plane curvature. For C/δ well above 1, in-plane curvature dominates, and the interface behaves as though in a Hele-Shaw cell, with little or no entrapment of the defending phase (see Fig. 2). Correspondingly, the areal saturation (S_f) at satiation ranges from about 0.37 ($C/\delta\gg 0$) to 1 ($C/\delta\gg 1$). In the intermediate range of C/δ ($\sim 1-10$), Glass *et al.* [15] also observed a nonunique behavior of S_f at satiation with respect to wetting versus nonwetting fluid invasions. This nonunique behavior is due to asymmetry in competition between the smoothing and roughening mechanisms, which results from the asymmetric distribution of $1/a$.

A useful model for k_{rs} should adequately describe behavior across the wide array of entrapped phase structures corresponding to the full range of C/δ. Nicholl *et al.* [7] proposed a model for k_{rs} that identified four controlling parameters: a tortuosity factor τ, the areal saturation of the flowing phase, S_f, and two parameters that quantify deviations in the mean and variance of the aperture field within the flowing phase from those in the entire fracture. They calculated values for each of these parameters for seven satiated phase structures, demonstrating that the tortuosity played the most significant role in determining k_{rs}. However, they did not develop relationships for predicting the model parameters based on fracture and fluid properties. We present an improved and general model that uses concepts from continuum percolation theory to develop a relationship between k_{rs} and S_f and explore this relationship over a broad range of C/δ. Our model leads to general predictive relationships for k_{rs} in terms of fracture and fluid properties. It is important to emphasize the distinction between this relationship and the more commonly used relative permeability-saturation relationship in two-phase flows. The latter involves relative permeabilities at different saturation values corresponding to a single invasion process. In contrast, the k_{rs}-S_f relationship does not correspond to a single invasion process. It represents the variation of (satiated) relative permeability k_{rs} with the areal saturation at satiation (S_f), which is in turn controlled by C/δ, the true "independent variable" in this context. The model predictions agree well with computational estimates of relative permeability obtained using flow simulations in partially saturated fractures.

II. MODEL FOR k_{rs}

Our approach is similar to that of Nicholl *et al.* [7], who proposed a theoretical expression for relative permeability in a variable-aperture fracture by modifying a result for the effective transmissivity of a heterogeneous two-dimensional medium [16] to account for impermeable obstructions to the flowing phase [17]. These theoretical expressions are approximations to the true effective transmissivity, in that they invoke the local cubic law, which assumes that pressure gradients across the aperture are negligible. However, Nicholl *et al.* [7] found that the relative permeability predicted by flow simulations based on the local cubic law were within 10% of experimentally measured relative permeabilities. This is evidently because the relative influence of the entrapped phase on the flow structure is substantially larger than the relative differences between the flow structure predicted by the three-

dimensional Stokes equations versus the local cubic law. Though Nicholl *et al.* [7] measured k_{rs} in a range of different phase structures, their experimental phase structures were not generated by systematic phase invasions. In particular, their phase structures did not cover the entire range of S_f corresponding to the full range of C/δ and thus did not present a complete picture of k_{rs}.

For a saturated variable-aperture fracture, the effective transmissivity can be obtained using a perturbation analysis on the flow equation:

$$\nabla \cdot [T(x,y)\, \nabla h(x,y)] = 0, \tag{3}$$

where $T(x,y)$ is the spatially variable transmissivity field and h refers to the head field. The local transmissivity based on the Reynolds equation is given by

$$T(x,y) = \frac{a^3(x,y)g}{12v}, \tag{4}$$

where $a(x,y)$ is the spatially variable-aperture field, g is the gravitational acceleration, and v is the kinematic viscosity of the fluid. Without making any assumptions about the specific distribution of $T(x,y)$ (except that it is positive), a perturbation analysis of Eq. (3) can be developed in terms of the scaled transmissivity variation $T'/\langle T\rangle$, where $\langle T\rangle$ is the mean transmissivity. The analysis begins from

$$\nabla \cdot \left[\langle T\rangle \left(1 + \frac{T'}{\langle T\rangle}\right) \nabla (\langle h\rangle + h') \right] = 0. \tag{5}$$

The effective transmissivity for saturated flow, denoted here by T_{sat}, is then quantified based on the relationship for the mean flux in terms of the mean gradient:

$$\langle q\rangle = -\langle T\, \nabla h\rangle = T_{sat}\langle -\nabla h\rangle.$$

In the case of small perturbations ($\delta \ll 1$), $T'/\langle T\rangle \approx 3a'/\overline{a}$ to first order in the aperture variations a' and the effective transmissivity for saturated flow in isotropic random aperture fields can be shown to be

$$T_{sat} = \frac{\langle a\rangle^3 g}{12v}(1 - 1.5\delta^2). \tag{6}$$

Expression (6) can also be obtained by a two-dimensional extension of a Landau-Lifshitz [16] analysis of the effective conductivity of a heterogeneous medium, as discussed by Zimmerman and Bodvarsson [17]. In the case of a lognormal aperture distribution with isotropic spatial correlation, a similar small-perturbation analysis based on $\ln(T)$ yields the result that the effective transmissivity is the geometric mean of the transmissivity field [18–20]. For this case, Eq. (6) is a consistent approximation to the geometric mean, to second order in δ.

For a partially saturated variable-aperture fracture, the effective transmissivity (denoted as T_p) can be represented by modifying Eq. (6) with an additional reduction factor due to the reduced area occupied by the flowing phase [7]:

$$T_p = k_{rs\|}\frac{\langle a_f\rangle^3}{12}(1 - 1.5\delta_f^2). \tag{7}$$

In Eq. (7), the subscript f refers to the flowing phase, so that $\langle a_f\rangle$ and δ_f, respectively, represent the mean and coefficient of variation of apertures in the region occupied by the flowing phase. Note that the volumetric saturation of the flowing fluid is equal to $S_f\langle a\rangle/\langle a_f\rangle$. The quantity $k_{rs\|}$ in Eq. (7) represents the reduction of permeability obtained in a parallel-plate fracture (or, equivalently, a homogeneous medium) with impermeable obstructions, whose geometries are identical to those of the entrapped phase.

We define the relative permeability as the ratio of Eq. (7) to Eq. (6):

$$k_{rs} = k_{rs\|}AB, \tag{8}$$

such that the total flow through a satiated fracture is represented by $Q = k_{rs}T_{sat}W\langle -\nabla h\rangle$, where W is the width of the fracture. In Eq. (8), A and B represent the influence of the relative change in the mean and coefficient of variation of the apertures occupied by the flowing phase from the corresponding values in a fully saturated fracture:

$$A = \langle a_f\rangle^3/\langle a\rangle^3, \quad B = (1 - 1.5\delta_f^2)/(1 - 1.5\delta^2). \tag{9}$$

As shown in the next section, the strongest contribution to k_{rs} is from $k_{rs\|}$, which is related to the entrapped phase geometry. The term A is next in order of importance and B has a very minor influence on k_{rs}. We outline approaches for quantifying each of these terms below.

Systematic simulations of $k_{rs\|}$ for a range of C/δ (presented in Sec. III) demonstrate that the behavior of $k_{rs\|}$ with respect to S_f is similar to that observed in continuum percolation problems (i.e., linear dependence on S_f near $k_{rs\|}=1$ and power dependence on S_f near $k_{rs\|}=0$); thus, we invoke concepts from continuum percolation to quantify $k_{rs\|}$. The typical continuum percolation problem considers percolation and conduction in a homogeneous medium with randomly positioned identical "holes" as the area fraction of the holes is varied. Thus the entrapped defending fluid phase at the satiated state in variable aperture fractures corresponds to the hole phase in continuum percolation. However, unlike in standard continuum percolation, the geometry of the entrapped phase here is irregular, and there is considerable variation in the size, shape, orientation and aspect ratios of individual entrapped regions [see Figs. 2(b)–2(e)]. The variation of conductivity with area fraction of the hole phase has been considered extensively for the case of holes with regular shapes, such as circles and ellipses, squares and rectangles, and needles [21–28]. In some studies of continuum percolation (e.g., [25]), mixtures of holes with different shapes and sizes have been considered, with the conclusion that a scaled percolation threshold (x_c in [25]) at which the conductivity goes to zero is almost invariant over a wide range of continuum percolation systems. Garboczi *et al.* [25] also proposed a universal conductivity curve for two-dimensional continuum percolation systems, involving the variable x, which is related to the remaining area fraction p (same as our S_f) as $p = \exp(-xA_h/L_{eff}^2)$, where A_h is the area

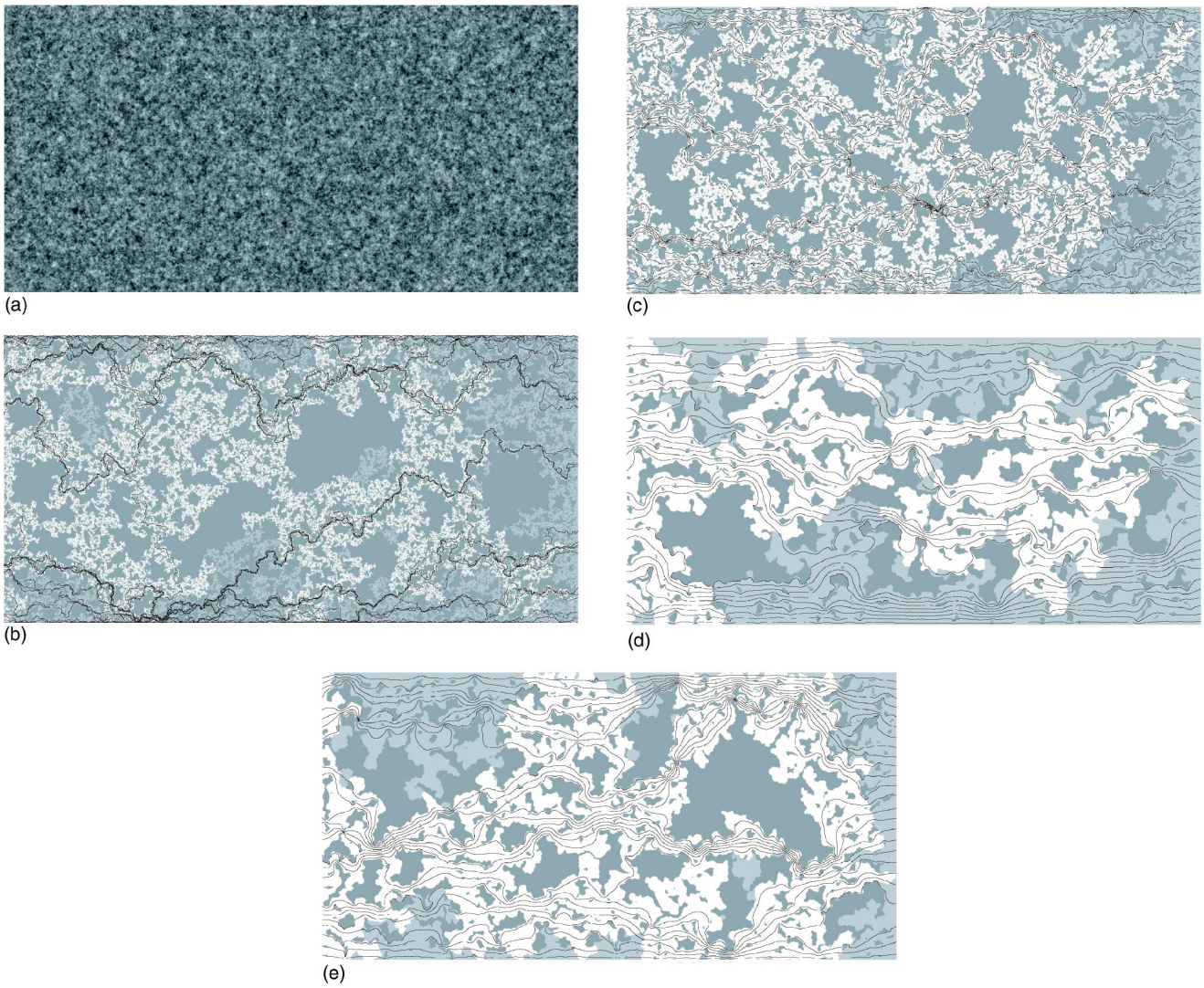

FIG. 2. Aperture field and example of satiated phase structure and flow paths: (a) Aperture field, grayscale depicts smaller apertures with darker shading; (b) wetting invasion, $C=0$, $\delta=0.0625$ (IP), $S_f \sim 0.38$; (c) wetting invasion, $C=0.0335$, $\delta=0.0625$, $C/\delta=0.536$, $S_f \sim 0.51$; (d) wetting invasion, $C=0.134$, $\delta=0.0625$, $C/\delta=2.144$, $S_f \sim 0.74$; and (e) nonwetting invasion, $C=0.134$, $\delta=0.0625$, $C/\delta=2.144$, $S_f \sim 0.69$. Invasion was from left to right; dark gray regions represent defending phase entrapped within the rough-walled fracture, white regions represent the location of the invading phase at breakthrough (i.e., percolation threshold), light gray regions represent additional locations occupied by the invading phase at satiation, and black shows the trajectory of 25 particles released along the inflow edge of the fracture. The initial particle spacing was flux weighted.

of a single "hole" and L_{eff} is a characteristic length defined based on the initial slope of the conductivity curve. Their universal conductivity curve is of the form

$$k_{rs\|} = \left[\frac{(1 - x/x^*)(1 + x/x^* + \alpha x^2 (t x_I - x^*)/t^2 x_I^2 x^*)}{(1 + x/x_I)} \right]^t. \tag{10}$$

In Eq. (10), x^* refers to the critical value of x at which the conductivity goes to zero, x_I is a parameter defining the initial slope ($k_{rs\|} \sim 1 - tx/x_I$ for x close to 0), α (=0.7) is a fitting parameter, and t is the conductivity exponent ($t=1.3$ in two dimensions).

Direct extension of Eq. (10) to the problem at hand is complicated by two factors: the wide distribution of the area A_h associated with a single hole, evident from the phase structures shown in Fig. 2, and the nonlinear relationship between S_f (or p) and x that will lead to a complicated expression for $k_{rs\|}$. We therefore considered a linearized relationship between S_f and x, where $-\ln[1-(1-S_f)] \approx 1 - S_f$ is proportional to x. This leads to relationships in terms of $1 - S_f$, rather than x; we note that Xia and Thorpe [24] also expressed their conductivity relationships in terms of $1 - S_f$ (their c). To further simplify the expression for $k_{rs\|}$, we dropped the last term in the numerator of Eq. (10), which also eliminates the fitting parameter (α), and modified the denominator to obtain a linear behavior of the form $k_{rs\|} \sim 1 - (1-S_f)/(1-S_{fI})$ for x close to 0, leading to

$$k_{rs\|} = \left[\left(1 - \frac{1-S_f}{1-S_f^*}\right)\left(1 + \frac{1-S_f}{1-S_f^*}\right) \Big/ \left(1 + \frac{1-S_f}{t(1-S_{fI})}\right) \right]^t. \tag{11}$$

In Eq. (11), there are three parameters: S_f^* is the percolation threshold at which $k_{rs\|}$ goes to zero, S_{fI} is the point where the initial slope for a small area fraction of holes crosses the abscissa when extrapolated, and t is the conductivity exponent, which has a value close to 1.3 in two dimensions [22,25–28]. Both S_f^* and S_{fI} depend on the aspect ratio of the holes in general [24,25]. Expression (11) is basically an interpolant that is consistent with critical behavior near the percolation threshold [$k_{rs\|} \sim (S_f - S_f^*)^t$ as S_f approaches S_f^*] and linear behavior for S_f near 1 [$k_{rs\|} \sim 1-(1-S_f)/(1-S_{fI})$], two limits that are universally observed for continuum percolation [24,25,28]. Although Eq. (10) was not originally developed for problems involving a wide range of sizes, shapes, and orientations of the hole phase, results in the next section show that the modified form (11) describes the behavior of $k_{rs\|}$ very well.

The secondary term in Eq. (8), A, represents the influence of the relative change in mean aperture within the flowing phase. Thus we expect $A>1$ for nonwetting fluid flow and $A<1$ for wetting fluid flow. A is also expected to depend strongly on δ, particularly for small values of C. For $C=0$ (IP in a correlated lattice), the fluid phase geometries do not vary with δ. However, because of selective occupancy of the aperture distribution, the mean aperture within the flowing phase, and thus A, will be influenced by δ. For standard percolation (SP), the invading phase occupies apertures strictly in ascending (wetting) or descending (nonwetting) order, which allows development of an analytical expression for A. However, this analytical expression does not provide satisfactory estimates of A for phase structures generated by MIP in two-dimensional variable-aperture fractures, where in-plane curvature effects lead to significant deviations from the assumption of sequential occupancy. Therefore, we propose an empirical relationship for A that is based on an analysis of aperture field statistics within the invading phase over a large number of invasion simulations (described in detail in the following section):

$$A = 1 \pm b\delta(1 - S_f)^2, \tag{12}$$

where b is a fitted parameter. The last term B in Eq. (8), which is a measure of the change in aperture variance from the saturated state to the satiated state, has a very minor influence, and thus we have not developed an analytical or empirical relationship to quantify the influence of B on k_{rs}.

III. EVALUATION OF THE k_{rs}-S_f MODEL

To evaluate the effectiveness of the model for k_{rs} proposed in the previous section, for use over a wide range of aperture-field statistics and fluid properties, we simulated flow through fractures containing phase structures generated from MIP simulations by systematically varying C/δ [15]. The aperture fields (1024×2048) used for the simulations were generated using a fast Fourier transform (FFT) algorithm, with a Gaussian aperture distribution and a power spectrum of the form

$$G(k_x, k_y) \propto (1 + l^2k_x^2 + l^2k_y^2)^{-n}, \tag{13}$$

where k_x and k_y are the wave numbers corresponding to the x and y dimensions, n is an exponent in the range $1 \leqslant n \leqslant 2$, and l is a cutoff length scale [29]. This general form of $G(k_x, k_y)$ is widely accepted as a reasonable model for natural fractures where the apertures exhibit a self-affine structure with Hurst exponent, $H=n-1$ for $|k|>1/l$ and negligible correlation for $|k|<1/l$ [30]. The functional form of G in Eq. (13) yields a smooth transition from power-law behavior ($|k|>1/l$) to the cutoff value ($|k|<1/l$) that results in random fields with well-behaved covariance functions (i.e., no oscillations as occur with an abrupt cutoff). We chose l to yield $\lambda=5$ grid blocks for fields with zero mean, variance of 1, and $n=1.3$, where λ is defined as the separation distance at which the semivariogram reaches a value of $\sigma_a^2(1-1/e)$. We generated six random fields and scaled each to yield fractures with $\delta=0.0625$, 0.125, and 0.25, resulting in a total of 18 aperture-field realizations [Fig. 2(a)]. Higher values of δ yielded contact areas where the aperture is zero, which introduced additional complications during phase invasion and will not be addressed here.

In each of the 18 aperture fields, Glass *et al.* [15] simulated wetting and nonwetting phase invasions using MIP for 14 values of C that began at 0, followed by 0.0021 with successive doubling up to 8.58, for a total of 504 simulations. The invading phase was supplied across the entire edge of one short side of the random field while the defending phase was allowed to leave the field through the other three sides. Defending phase trapping was implemented and the simulation ended when all sites were either filled with invading phase or entrapped defending phase. The results of the phase invasion simulations allow direct measurements of S_f, A, and B, but estimating k_{rs} and $k_{rs\|}$ requires flow simulations in the fractures.

We simulated flow within the satiated phase structures by solving a finite-difference representation of Eq. (3) in each aperture-phase distribution field. We specified no-flux boundary conditions at the interfaces between the flowing and entrapped phases, with uniform constant pressure boundaries along the two short edges of the fractures and no flow boundaries along the long edges. The ratio of the simulated flowrate in the satiated fracture to that in the saturated fracture provides an estimate of k_{rs} for a fracture occupied by a specific phase distribution. Similar computations in a hypothetical parallel-plate fracture with impermeable obstructions corresponding to the entrapped phase geometry led to estimates of $k_{rs\|}$.

IV. RESULTS

The results of the flow simulations demonstrate the influence of the entrapped phase on flow through satiated fractures. Figures 2(b)–2(e) show stream lines through fractures at several values of C/δ after both wetting and nonwetting invasions. For $C/\delta=0$ [Fig. 2(b)], the flowing phase occupies a small fraction of the total area, and the complex entrapped-

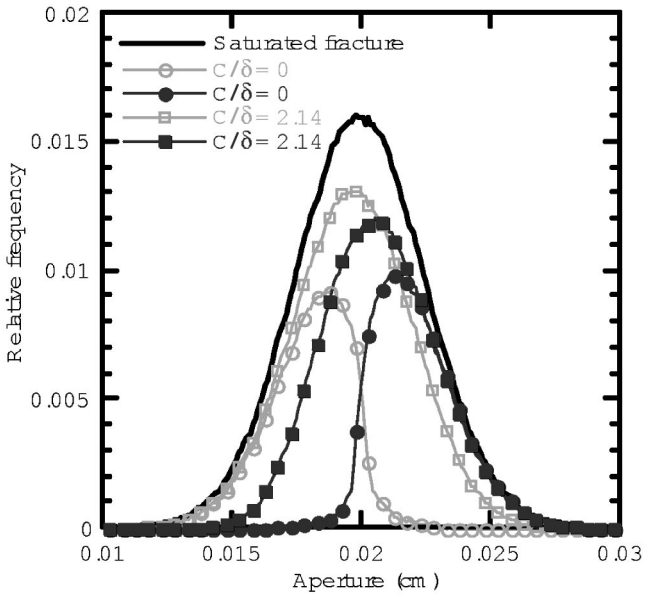

FIG. 3. Distributions of apertures occupied by the invading phase at satiation for both wetting (open symbols) and nonwetting (solid symbols) invasions. The thick solid line represents the aperture distribution for the saturated fracture.

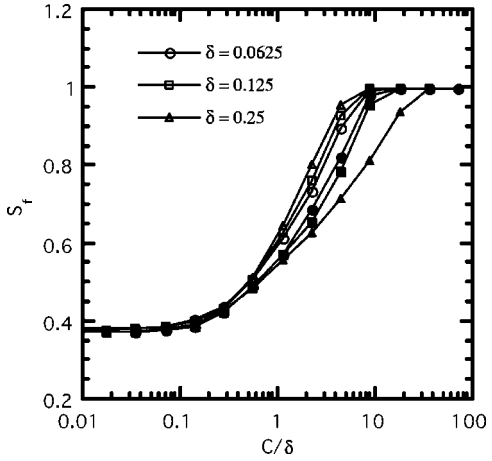

FIG. 4. Average S_f for six realizations plotted against C/δ for both wetting (open symbols) and nonwetting (solid symbols) invasions.

phase structures result in large regions of flowing phase capturing very little of the total flow through the fracture. This is particularly evident in the center of the fracture where several large entrapped regions nearly block flow. As C/δ increases [Figs. 2(c) and 2(d)], the regions of entrapped defending phase become more compact, leading to a larger number of open flow paths through the center of the fracture, less tortuous streamlines, and increased k_{rs}. Fundamental differences in the entrapped phase result during wetting and nonwetting invasions due to the order in which apertures are filled along the invading interface. Figures 2(d) and 2(e) demonstrate that wetting and nonwetting invasions at the same values of C and δ lead to different entrapped regions within the same aperture field. Furthermore, S_f is larger for the wetting invasion than the nonwetting invasion, which leads to slightly more tortuous stream lines for the nonwetting invasion.

The distributions of the apertures occupied by the invading fluid at satiation vary significantly for wetting versus nonwetting invasions (Fig. 3). For small values of C/δ there is little overlap between the distributions corresponding to the wetting and nonwetting invasions and they are almost symmetric about the mean aperture of the saturated fracture ($\langle a\rangle = 0.02$ cm). However, as C/δ increases, the amount of overlap increases as a result of enhanced interface smoothing during invasion. Also, at larger values of C/δ, the distributions are no longer symmetric about $\langle a\rangle$. This asymmetry is due to the asymmetric distribution of $1/a$ that corresponds to a Gaussian distribution for a. Because aperture-induced capillary pressure, which influences phase invasion, is proportional to $1/a$, asymmetry in the $1/a$ distribution leads to different behavior along the invading interface for wetting and nonwetting invasions. With a symmetric distribution for $1/a$, the aperture distributions for wetting and nonwetting invasions should be symmetric about $\langle a\rangle$ for all values of C and δ.

To evaluate the ability of the model presented in Eq. (8) to predict k_{rs}, we calculated the relevant parameters obtained from the 504 flow simulations. To clarify presentation of the data, for each combination of C and δ we show only the average parameter values from the 6 aperture-field realizations in the following plots. For each parameter, the standard deviation across the 6 realizations was no larger than 11% of the mean value and was typically less than 5%. This demonstrates that the influence of C/δ on these parameters is more significant than variability across realizations. Figure 4 shows S_f plotted against C/δ and shows, as detailed by Glass *et al.* [15], that S_f exhibits a unique relationship with C/δ for small values of C/δ. At larger values of δ and C/δ above ~ 0.5, measured values of S_f fan apart and then converge again at large values of C/δ. Glass *et al.* [15] explained this envelope based on the asymmetry in competition between smoothing and roughening, which is related to the asymmetric distribution of $1/a$. Based on the relationship between C/δ and S_f in Fig. 4 a relationship that effectively quantifies k_{rs} as a function of S_f may be further generalized to directly relate k_{rs} to C/δ.

The distribution of apertures occupied by the invading fluid during wetting and nonwetting invasions (Fig. 3) strongly influences measured values of A. In each aperture field-realization, A was determined at each value of δ and S_f by computing the mean aperture value from pixels occupied by the flowing phase. Figure 5 shows A plotted against S_f with the results of fitting Eq. (12) to the data. The asymmetry in the distributions of aperture occupied by the invading fluid for the wetting and nonwetting invasions (Fig. 3) results in different values for the fitted parameter b: for nonwetting invasions $b = 4.59$ and for wetting invasions $b = 3.98$. The fitted curves for the wetting invasions deviate slightly from the data for intermediate values of S_f, but fit the data well for small values of S_f where A has the largest influence on estimates of k_{rs}.

Figure 6 shows $k_{rs\|}$ plotted against S_f for all values of C/δ and compares these results to Eq. (11), the proposed model

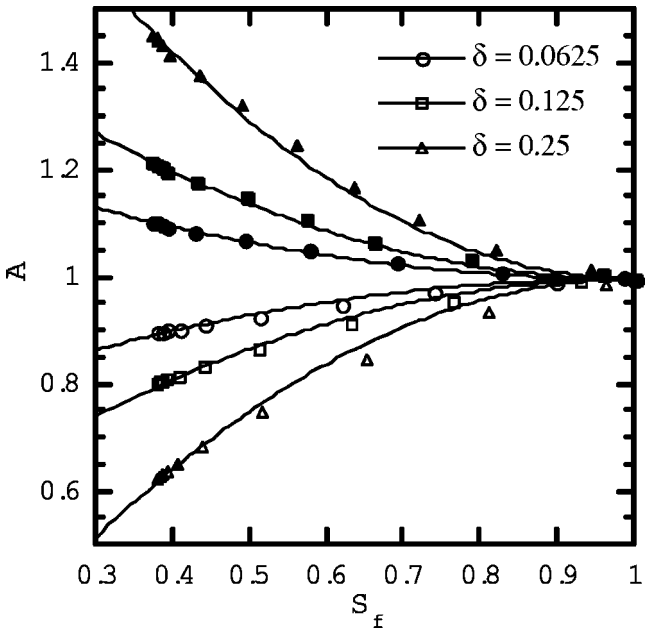

FIG. 5. A plotted against S_f for all values of δ for both wetting (open symbols) and nonwetting (solid symbols) invasions.

of $k_{rs\|}(S_f)$, with values of $S_{fI}=0.72$, $S_f^*=0.333$, and $t=1.3$. The model fits the simulated values of $k_{rs\|}$ quite well across the full range of S_f and only slightly overestimates the simulated values in the range of $0.55<S_f<0.85$. The value of 0.72 for the parameter S_{fI}, which is related to the initial slope, was obtained based on a linear fit to simulated $k_{rs\|}$ near $S_f=1$. With $t=1.3$, $S_f^*=0.333$ adequately represents the behavior of the simulated $k_{rs\|}$ values for the smallest values of S_f. In continuum percolation theory, S_f^* corresponds the critical value at which $k_{rs\|}$ goes to zero and, in the context of satiated phase structures, represents an absolute lower bound

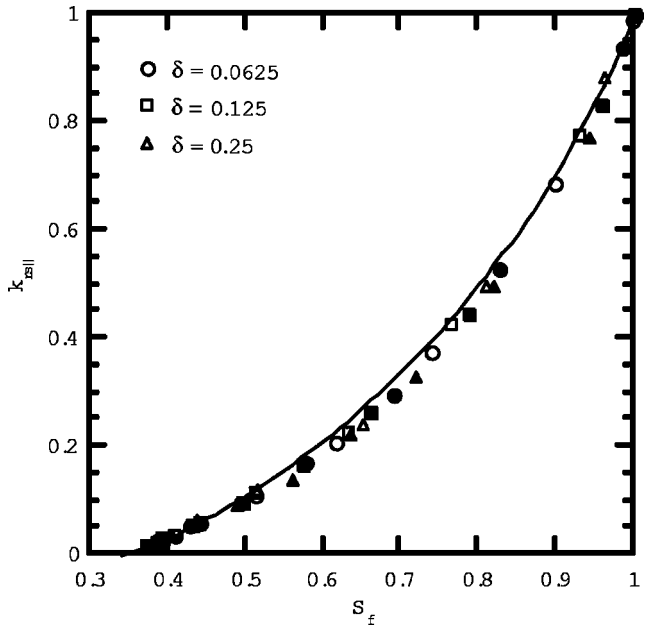

FIG. 6. $k_{rs\|}$ plotted against S_f for all values of δ for both wetting (open symbols) and nonwetting (solid symbols) invasions.

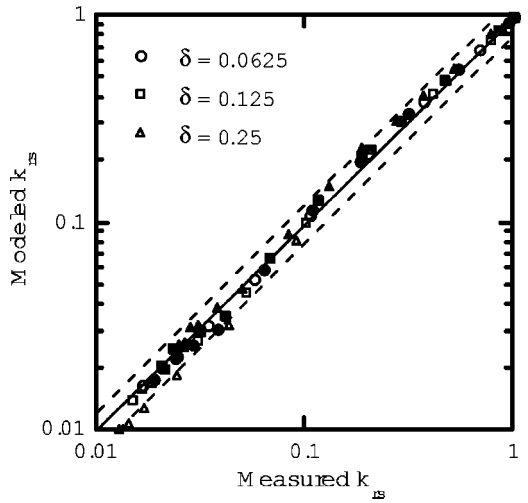

FIG. 7. k_{rs} measured from flow simulations plotted against k_{rs} estimated using Eq. (8) for both wetting (open symbols) and nonwetting (solid symbols) invasions. The dashed lines represent the ±20% discrepancy bounds between the measured and modeled results.

for S_f at satiation. All satiated phase structures must correspond to $S_f>S_f^*$; the lowest value observed in MIP simulations over numerous realizations of random aperture fields was 0.34 at the limit of $C/\delta=0$ (the mean value for $C/\delta=0$ over 36 realizations is 0.37). It is important to distinguish the above interpretation of S_f^* from the value of S_f at first breakthrough during MIP, which is as low as 0.23 for $C/\delta=0$ and around 0.8 at large values of C/δ. It is interesting to note that the value of 0.333 for S_f^* corresponds to the percolation threshold for continuum percolation with circular or square holes [21,25,31], although the actual geometry of the entrapped phase (see Fig. 1) is much more complicated, involving a wide range of sizes, shapes, orientations, and aspect ratios. Garboczi *et al.* [25] investigated the variation of percolation threshold in mixed systems with circles of two different diameters, needles with two different lengths, and circle-needle mixtures. Their results showed minor variations in the scaled percolation threshold about their proposed universal value. We are unaware of any systematic results for continuum percolation with a broad distribution of size, shape, and aspect ratios for the holes, for comparison with our estimate of S_f. This and the explanation for why Eq. (11) provides an excellent model for $k_{rs\|}$ despite the complexity of the entrapped phase structure appear to be interesting problems for further research.

Using Eqs. (11) and (12) to model $k_{rs\|}$ and A over the range of S_f and δ allows us to use Eq. (8) to estimate k_{rs} over the full range of parameters. Figure 7 compares the simulated values of k_{rs} to estimates using Eq. (8). The discrepancies between the simulated results and the modeled estimates of k_{rs} increase with δ, the largest of which are around a 25% difference between the modeled and simulated estimates of k_{rs}. The largest discrepancies occur for the wetting invasion at $\delta=0.25$ for $k_{rs}<0.05$ and for the nonwetting invasion at $\delta=0.25$ for $k_{rs}=0.19$. For smaller values of δ, the discrepancies all fall well within the 20% bounds shown in Fig. 7.

V. SUMMARY

We have developed a model for predicting the satiated relative permeability across a broad range of entrapped phase structures in variable aperture fractures. These entrapped phase structures represent both wetting and nonwetting displacements over a full spectrum of possible Curvature numbers (C) and a comprehensive set of fracture aperture statistics (δ). The resulting entrapped phase ranged from highly tortuous structures resulting from capillary fingering to compact smooth structures at large values of C/δ. The satiated relative permeability (k_{rs}) was shown to depend on the product of $k_{rs\|}$, which quantifies the influence of the phase geometry alone, with A, which accounts for the modification of the mean aperture due to the selective occupancy of the flowing phase.

Our model for the satiated relative permeability (k_{rs}) uses well-established ideas from continuum percolation theory to relate $k_{rs\|}$ with S_f. This generalized model for $k_{rs\|}$ exhibits a power function dependence on S_f near S_f^* (the percolation threshold) and linear behavior near $S_f=1$. The exponent in the power-function behavior at low S_f is consistent with the universal conductivity exponent (1.3) for two-dimensional percolation systems. The influence of aperture distribution and the effect of wetting versus nonwetting invasions on the mean aperture in the flowing phase are quantified through the term A. We have proposed a robust empirical relationship for A in terms of S_f and δ. As expected, A is greater than 1 for the nonwetting case and less than 1 for the wetting case and deviations from 1 are amplified by δ. Thus, for a given value of S_f, k_{rs} will be larger for flow of a nonwetting fluid than for a wetting fluid, with the difference enhanced at small values of S_f and large values of δ.

Comparison of the semiempirical model for k_{rs} to measurements of k_{rs} resulting from flow simulations through six fracture realizations over a range of C and δ demonstrates that the model predicts k_{rs} quite well over the full range of parameters. It is somewhat surprising that the influence of the complex phase structures on permeability can be quantified as a function S_f, a simple measure of the phase structure. However, it is likely that efforts to model other processes, such as solute transport in the flowing phase [32] or entrapped phase dissolution [8], will require higher-order measures of the entrapped phase geometry. We note that the model relates k_{rs} to δ and S_f, which in turn is fundamentally controlled by C/δ for the case of capillary-dominated displacements. Thus, for capillary-dominated displacements in a given fracture it is possible to estimate k_{rs} directly if the fracture aperture statistics and contact angle at the interface (i.e., C, δ, and α) are known.

ACKNOWLEDGMENTS

Funding for this work was provided by the Department of Energy's Office of Basic Energy Sciences, Geosciences Program under Contract Nos. DE-FG03-96ER14590 (University of Colorado), DE-AC04-94AL85000 (Sandia National Laboratories), and W-7405-Eng-48 (Lawrence Livermore National Laboratory).

[1] K. Pruess and Y. W. Tsang, Water Resour. Res. **26**, 1915 (1990).
[2] M. Fourar, S. Bories, R. Lenormand, and P. Persoff, Water Resour. Res. **29**, 3699 (1993).
[3] J. R. Murphy and N. R. Thomson, Water Resour. Res. **29**, 3453 (1993).
[4] P. Persoff and K. Pruess, Water Resour. Res. **31**, 1175 (1995).
[5] D. Wilkinson and J. F. Willemsen, J. Phys. A **16**, 3365 (1983).
[6] R. J. Glass, L. Yarrington, and M. J. Nicholl, Water Resour. Res. **34**, 3215 (1998); Water Resour. Res. **36**, 1991 (2000).
[7] M. J. Nicholl, H. Rajaram, and R. J. Glass, Geophys. Res. Lett. **27**, 393 (2000).
[8] L. R. Zhong, A. Mayer, and R. J. Glass, Water Resour. Res. **37**, 523 (2001).
[9] R. L. Detwiler, H. Rajaram, and R. J. Glass, Water Resour. Res. **37**, 3115 (2001).
[10] S. E. Dickson and N. R. Thomson, Environ. Sci. Technol. **37**, 4128 (2003).
[11] R. Chandler, J. Koplik, K. Lerman, and J. F. Willemsen, J. Fluid Mech. **119**, 249 (1982).
[12] M. M. Dias and D. Wilkinson, J. Phys. A **19**, 3131 (1986).
[13] H. Amundsen, G. Wagner, U. Oxaal, P. Meakin, J. Feder, and T. Jossang, Water Resour. Res. **35**, 2619 (1999).
[14] G. Wagner, P. Meakin, J. Feder, and T. Jossang, Physica A **264**, 321 (1999).
[15] R. J. Glass, H. Rajaram, and R. L. Detwiler, Phys. Rev. E **68**, 061110 (2003).
[16] L. D. Landau and E. M. Lifshitz, *Electrodynamics of Continuous Media* (Pergamon, New York, 1960).
[17] R. W. Zimmerman and G. S. Bodvarsson, Transp. Porous Media **23**, 1 (1996).
[18] A. L. Gutjahr, L. W. Gelhar, A. A. Bakr, and J. R. Macmillan, Water Resour. Res. **14**, 953 (1978).
[19] G. Dagan, Water Resour. Res. **15**, 47 (1979).
[20] L. W. Gelhar, *Stochastic Subsurface Hydrology* (Prentice-Hall, Englewood Cliffs, NJ, 1993).
[21] G. E. Pike and C. H. Seager, Phys. Rev. B **10**, 1421 (1974).
[22] B. I. Halperin, S. Feng, and P. N. Sen, Phys. Rev. Lett. **54**, 2391 (1985).
[23] S. Feng, B. I. Halperin, and P. N. Sen, Phys. Rev. B **35**, 197 (1987).
[24] W. Xia and M. F. Thorpe, Phys. Rev. A **38**, 2650 (1988).
[25] E. J. Garboczi, M. F. Thorpe, M. S. Devries, and A. R. Day, Phys. Rev. A **43**, 6473 (1991).
[26] D. Stauffer and A. Aharony, *Introduction to Percolation Theory*, 2nd ed. (Taylor & Francis, London, 1992).
[27] M. Sahimi, *Flow and Transport in Porous Media and Fractured Rock* (VCH, Weinheim, 1995).

[28] J. Tobochnik, M. A. Dubson, M. L. Wilson, and M. F. Thorpe, Phys. Rev. A **40**, 5370 (1989).
[29] S. R. Brown, J. Geophys. Res. **100**, 5941 (1995).
[30] P. M. Adler and J.-F. Thovert, *Fractures and Fracture Networks* (Kluwer, Boston, 2000).
[31] E. T. Gawlinski and H. E. Stanley, J. Phys. A **14**, L291 (1981).
[32] R. L. Detwiler, H. Rajaram, and R. J. Glass, Geophys. Res. Lett. **29**, 1 (2002).